

Distribution-Level AirComp for Wireless Federated Learning under Data Scarcity and Heterogeneity

Jun-Pyo Hong, *Member, IEEE*, Hyowoon Seo, *Member, IEEE*, and Kisong Lee, *Senior Member, IEEE*,

Abstract—Federated Learning (FL) has gained considerable attention as a privacy-preserving and localized approach to implementing edge artificial intelligence (AI). However, conventional FL methods face critical challenges in realistic wireless edge networks, where training data is both limited and heterogeneous, often leading to unstable training and poor generalization. To address these challenges in a principled manner, we propose a novel wireless FL framework grounded in Bayesian inference. By virtue of the Bayesian approach, our framework captures model uncertainty by maintaining distributions over local weights and performs distribution-level aggregation of local distributions into a global distribution. This mitigates local overfitting and client drift, thereby enabling more reliable inference. Nevertheless, adopting Bayesian FL increases communication overhead due to the need to transmit richer model information and fundamentally alters the aggregation process beyond simple averaging. As a result, conventional Over-the-Air Computation (AirComp), widely used to improve communication efficiency in standard FL, is no longer directly applicable. To overcome this limitation, we design a dedicated AirComp scheme tailored to Bayesian FL, which efficiently aggregates local posterior distributions at the distribution level by exploiting the superposition property of wireless channels. In addition, we derive an optimal transmit power control strategy, grounded in rigorous convergence analysis, to accelerate training under power constraints. Our analysis explicitly accounts for practical wireless impairments such as fading and noise, and provides theoretical guarantees for convergence. Extensive simulations validate the proposed framework, demonstrating significant improvements in test accuracy and calibration performance over conventional FL methods, particularly in data-scarce and heterogeneous environments.

Index Terms—Wireless federated learning, over-the-air computation, Bayesian learning, variational inference, data scarcity, non-i.i.d. data, convergence analysis

I. INTRODUCTION

FEDERATED learning (FL) has emerged as a promising privacy-preserving paradigm for collaboratively training machine learning models across decentralized data sources. Instead of transmitting raw data to a central server, FL allows clients to retain their local data and only exchange model updates, thereby mitigating privacy risks. A widely adopted baseline in this framework is Federated Averaging (FedAvg) [1], where clients iteratively train local models and upload

them for global averaging. Despite its simplicity and scalability, practical FL systems often suffer from statistical heterogeneity—client data are typically non-identically distributed (non-i.i.d.) and imbalanced, reflecting personal usage patterns or localized sensing environments.

This inherent heterogeneity induces client drift, where local updates diverge from the global objective, particularly when local models are trained for multiple steps without coordination. Consequently, the aggregated model may converge slowly or even degrade in performance compared to centralized training [2]. To counteract this, various extensions to FedAvg have been proposed. For example, FedProx [3] introduces a proximal regularization term to restrict local model deviation, and SCAFFOLD [4] employs control variates to reduce variance in gradient estimation. FedNova [5] normalizes update lengths to account for client-specific training effort, while MOON [6] and FedDyn [7] adopt contrastive and dynamic regularization, respectively.

These methods effectively mitigate client drift and improve fairness across clients. However, they implicitly assume that each client holds a sufficiently large and representative dataset. In domains such as healthcare, biomedical sensing, smart homes, robotics, and cybersecurity, this assumption often breaks down. Clients may have access to only a handful of samples, and their data distributions can vary drastically. Under such data scarcity and strong non-i.i.d. conditions, local models exhibit high variance, exacerbating drift and leading to unstable or overfitted global models [8]. Inadequate sample coverage further impairs uncertainty calibration, yielding overconfident predictions with poor generalization.

Bayesian FL has recently gained traction as a principled approach to address these challenges. Unlike deterministic methods, Bayesian FL maintains a distribution over model weights rather than a single point estimate, enabling explicit modeling of epistemic uncertainty across clients and during aggregation [9]. Each client estimates a local posterior over model parameters using its data, and the server aggregates these posteriors into a global one. Notably, [10] proposes forming the global posterior by multiplying local posteriors, yielding a distribution that minimizes the average Kullback-Leibler (KL) divergence from all local posteriors. This posterior conflation captures the diversity of learned models, regularizes training under limited data, and improves generalization in heterogeneous settings.

Despite its theoretical advantages, Bayesian FL poses significant practical challenges. In particular, each client must transmit richer information—typically the mean and variance of its posterior—effectively doubling the communication

J.-P. Hong is with the School of Electronics and Electrical Engineering, Hongik University, Seoul 04066, South Korea (e-mail: jp_hong@hongik.ac.kr).

H. Seo is with the Department of Electrical and Computer Engineering, Sungkyunkwan University, Gyeonggi-Do 16419, South Korea (e-mail: hyowoonseo@skku.edu).

K. Lee is with the Department of Information and Communication Engineering, Dongguk University, Seoul 04620, South Korea (e-mail: klslee851105@gmail.com).

(Corresponding authors: Hyowoon Seo and Kisong Lee)

payload compared to standard FL. This overhead becomes prohibitive in wireless edge networks, where communication bandwidth is limited and channel conditions are dynamic. Moreover, existing Bayesian FL studies generally neglect the communication bottleneck, limiting their applicability in real-world systems.

To address the communication inefficiency, over-the-air computation (AirComp) has emerged as a promising technique for scalable FL in wireless networks. AirComp leverages the waveform superposition property of wireless channels to compute functions—such as model averages—directly in the analog domain. Specifically, clients simultaneously transmit their local updates over a shared channel, and the server receives a superimposed signal that approximates the aggregated result. This process inherently supports linear aggregation and avoids the need for orthogonal transmissions, thereby reducing bandwidth consumption, especially in dense client scenarios [11], [12]. Enhancements such as power control and quantization techniques have further improved AirComp performance in practical deployments [13]–[18].

However, existing AirComp FL schemes have primarily focused on deterministic model updates (e.g., gradients or weights), and their integration with Bayesian FL remains largely unexplored. Some recent works [19]–[21] have adopted Bayesian tools for denoising or regularization in analog aggregation, but these methods do not learn or aggregate true posterior distributions over model parameters. As such, the benefits of Bayesian uncertainty modeling have yet to be fully realized in communication-efficient FL.

In this paper, we propose a distribution-level AirComp framework that enables communication-efficient and reliable Bayesian FL in wireless edge networks characterized by non-i.i.d. and data-scarce client datasets. Unlike FedAvg, which aggregates scalar parameters, our framework aggregates entire posterior distributions. We focus on the practical case where clients use variational inference to obtain Gaussian variational posteriors. The aggregation is performed through posterior conflation, where the mean of the global posterior is precision-weighted across clients, and its variance decreases accordingly, reflecting higher certainty.

To implement this conflation via AirComp, we introduce a tailored analog encoding scheme: each client encodes and transmits the sufficient statistics (mean and variance parameters) of its posterior over the wireless channel. The server then reconstructs the global posterior by applying appropriate de-biasing and normalization to the received superimposed signals. Our method integrates Bayesian learning and analog communication in a unified manner, preserving uncertainty quantification while drastically reducing communication overhead.

Through theoretical analysis and empirical validation, we demonstrate that the proposed framework maintains robust learning performance under severe data heterogeneity and scarcity, while offering substantial communication gains over existing Bayesian FL approaches.

In summary, our key contributions are as follows:

- *AirComp for Bayesian Posterior Aggregation*: We propose a novel AirComp framework that performs

distribution-level aggregation for Bayesian FL in the presence of data scarcity and heterogeneity. Each client transmits two precision-weighted statistics of its mean-field Gaussian posterior. Their superposition in the wireless channel implicitly computes the *product-of-Gaussians* conflation, allowing the server to recover the global posterior with a single post-processing step. This design enables uplink communication in constant time, regardless of the number of participating clients.

- *Convergence Analysis under Wireless Impairments*: We present the first convergence analysis for Bayesian FL with AirComp, explicitly capturing the impacts of wireless fading, additive channel noise, and update distortion. Theoretical guarantees are provided under channel impairments and constrained transmit power. The analysis reveals that, after a large number of training rounds, the distortion in aggregated updates becomes the dominant factor hindering convergence.
- *Optimized Power Control*: Based on our convergence analysis, we develop a power control strategy to accelerate training. The transmission power is optimized to minimize the aggregated update distortion at the BS by compensating for channel fading, local data imbalance, and limited power budget. Since the optimal power expression is derived in closed form, the influence of system parameters on system behaviors can be explicitly characterized.
- *Improved Uncertainty Calibration*: In scenarios where inference performance is limited by data scarcity, uncertainty calibration becomes a key metric for evaluating the reliability of predictions. The proposed framework delivers *well-calibrated* predictive probabilities through probabilistic inference. Empirically, our models achieve almost 50% lower expected calibration error (ECE) and yield reliability diagrams that are more closely aligned with ideal confidence levels, compared to conventional FL methods with AirComp. The provision of reliable confidence scores facilitates principled decision-making, making our framework particularly attractive for safety-critical applications such as home security and healthcare.

The rest of the paper is organized as follows. Section II provides background and preliminaries for Bayesian learning and its application in the federated setting. Section III introduces the system model and motivates the proposed framework. Section IV presents the proposed AirComp framework for Bayesian FL. Section V presents the convergence analysis and an optimized power control method to accelerate training. Section VI presents the simulation results, and Section VII concludes the paper.

II. BACKGROUND & PRELIMINARIES

A. Variational Bayesian Method

Contrary to standard (frequentist) machine learning, which focuses on deriving the best point estimate of model weights from data, Bayesian learning treats weights as random variables and focuses on deriving their distributions using prior

information and observed data. Specifically, Bayesian learning aims to determine the posterior distribution of the model weights $\mathbf{w} \in \mathbb{R}^d$, representing updated beliefs about these weights after taking into account the evidence provided by the data. For a given dataset \mathcal{D} , the posterior distribution is computed using Bayes' rule, which updates our beliefs about the model weights by combining the likelihood of the data with the prior distribution as

$$p(\mathbf{w}|\mathcal{D}) = \frac{p(\mathcal{D}|\mathbf{w})p(\mathbf{w})}{p(\mathcal{D})}. \quad (1)$$

The posterior distribution reflects beliefs about a range of possible model weights, making Bayesian methods more robust with limited data and better suited for estimating uncertainty—challenges not directly addressed by frequentist machine learning approaches. However, deriving the exact posterior distribution for general deep neural network (DNN) models is computationally challenging due to the high-dimensional integration required to calculate the evidence, $p(\mathcal{D}) = \int p(\mathcal{D}|\mathbf{w})p(\mathbf{w})d\mathbf{w}$.

To circumvent this challenge, several practical techniques have been developed to estimate or approximate the posterior distribution, including Monte Carlo Markov Chain (MCMC), variational inference, and Laplace approximation. Among these, we focus on employing variational inference, which enables computationally efficient and scalable local posterior approximation. Variational inference derives the parameterized distribution $q_{\theta^*}(\mathbf{w})$ that most closely approximates the true posterior distribution through the following optimization:

$$\begin{aligned} \theta^* &= \arg \min_{\theta \in \mathbb{R}^b} \text{KL}[q_{\theta}(\mathbf{w})\|p(\mathbf{w}|\mathcal{D})] \\ &= \arg \min_{\theta \in \mathbb{R}^b} \text{KL}[q_{\theta}(\mathbf{w})\|p(\mathbf{w})] - \mathbb{E}_{q_{\theta}(\mathbf{w})}[\log p(\mathcal{D}|\mathbf{w})] \quad (2) \\ &= \arg \min_{\theta \in \mathbb{R}^b} L_{\text{VI}}(\theta), \quad (3) \end{aligned}$$

where $\text{KL}[f(\mathbf{w})\|g(\mathbf{w})] = \int_{\mathbf{w}} f(\mathbf{w}) \log \frac{f(\mathbf{w})}{g(\mathbf{w})}$ denotes Kullback-Leibler (KL) divergence of the probability distribution $f(\mathbf{w})$ from $g(\mathbf{w})$, the log likelihood $\log p(\mathcal{D}|\mathbf{w})$ becomes $\sum_{(x,y) \in \mathcal{D}} \log p(y|x, \mathbf{w})$ for supervised learning, and $L_{\text{VI}}(\theta) = \text{KL}[q_{\theta}(\mathbf{w})\|p(\mathbf{w})] - \mathbb{E}_{q_{\theta}(\mathbf{w})}[\log p(\mathcal{D}|\mathbf{w})]$ is referred to as the variational free energy or the negative evidence lower bound (ELBO). To facilitate computing the expectation with respect to $q_{\theta}(\mathbf{w})$, the negative ELBO is approximated by

$$L_{\text{VI}}(\theta) \approx \sum_m^M \log q_{\theta}(\mathbf{w}_{(m)}) - \log p(\mathbf{w}_{(m)}) - \log p(\mathcal{D}|\mathbf{w}_{(m)}), \quad (4)$$

where $\mathbf{w}_{(m)}$ denotes the m -th Monte Carlo (MC) sample drawn from the distribution $q_{\theta}(\mathbf{w})$. Then, stochastic gradient descent (SGD) can be applied directly to (4) to solve the optimization problem (3) [22]–[24].

Specifically, for a Gaussian variational distribution under a mean-field approximation, the variational parameters consist of a mean vector and a diagonal covariance matrix, $\theta = (\boldsymbol{\mu}, \boldsymbol{\Sigma})$. To compute the approximate loss in (4), a MC sample $\mathbf{w}_{(m)}$ is drawn via the reparameterization $\mathbf{w}_{(m)} = \boldsymbol{\mu} + \boldsymbol{\Sigma}\boldsymbol{\epsilon}$, where $\boldsymbol{\epsilon} \sim \mathcal{N}(0, \mathbf{I}_d)$.

B. Bayesian FL

For a given set of edge devices $\mathcal{K} = \{1, 2, \dots, K\}$ and their distributed local datasets $\{\mathcal{D}_1, \mathcal{D}_2, \dots, \mathcal{D}_K\}$, the goal of Bayesian FL is to derive the posterior distribution of the model weights $\mathbf{w} \in \mathbb{R}^d$ toward the global dataset $\mathcal{D} = \bigcup_{k \in \mathcal{K}} \mathcal{D}_k$, denoted as $p(\mathbf{w}|\mathcal{D})$. However, it is infeasible to directly evaluate $p(\mathbf{w}|\mathcal{D})$ with the distributed local datasets. To address this limitation in the FL setup, the global posterior distribution can be estimated by collecting locally computed posterior distributions, $\{p(\mathbf{w}|\mathcal{D}_k)\}_{k \in \mathcal{K}}$, from devices and conflating them into a single representative distribution [10].

Suppose variational inference is employed by each device to approximate its local posterior distribution. At the beginning of training round t , the server disseminates the global variational posterior distribution $q_{\theta_t}(\mathbf{w})$ to all devices. Each device $k \in \mathcal{K}$ then performs local training on its dataset \mathcal{D}_k , treating the global posterior distribution as a prior in (3). In other words, the variational parameters $\theta_{t,k}$ locally trained at device k is obtained by solving the following optimization problem:

$$\begin{aligned} \theta_{t,k} &= \arg \min_{\theta \in \mathbb{R}^b} \lambda \text{KL}[q_{\theta}(\mathbf{w})\|q_{\theta_t}(\mathbf{w})] - \mathbb{E}_{q_{\theta}(\mathbf{w})}[\log p(\mathcal{D}_k|\mathbf{w})] \\ &= \arg \min_{\theta \in \mathbb{R}^b} L_k(\theta), \quad (5) \end{aligned}$$

where $L_k(\theta) = \lambda \text{KL}[q_{\theta}(\mathbf{w})\|q_{\theta_t}(\mathbf{w})] - \mathbb{E}_{q_{\theta}(\mathbf{w})}[\log p(\mathcal{D}_k|\mathbf{w})]$, and λ denotes a positive constant that regulates the degree of deviation from the global posterior distribution during local training. After completing the local training process defined by (5), each device k reports its locally updated variational parameters $\theta_{t,k}$ to the server. The server then aggregates these updates and refines the global posterior distribution by conflating the local variational posterior distributions $\{q_{\theta_{t,k}}(\mathbf{w})\}_{k \in \mathcal{K}}$. In large classes of distributions, including the Gaussian distribution, the conflated distribution that minimizes Shannon information loss is formed by the normalized product of the local distributions [25]. Assuming a Gaussian variational distribution, the global posterior distribution is updated as

$$\begin{aligned} p(\mathbf{w}|\mathcal{D}) &\hat{=} q_{\theta_{t+1}}(\mathbf{w}) \\ &= C \prod_{k \in \mathcal{K}} q_{\theta_{t,k}}(\mathbf{w})^{\pi_k}, \quad (6) \end{aligned}$$

where $\pi_k = |\mathcal{D}_k|/|\mathcal{D}|$, and C denotes a normalization constant. Once the global posterior distribution is refined, training proceeds to round $t + 1$. Consequently, the global posterior distribution is improved through the iterative aggregation and dissemination over multiple training rounds.

Although Bayesian approaches in [10], [26], [27] have been introduced to mitigate training performance degradation under non-i.i.d. data by incorporating probabilistic modeling, the impact of limited communication capacity on training performance and potential strategies to address this challenge remain unexplored. Updating the global posterior distribution at the server relies on the received local variational parameters $\{\theta_{t,k}\}_{k \in \mathcal{K}}$, making the design of efficient transmission schemes for parameter aggregation essential in practical wireless networks. Such efficiency not only reduces the required communication overhead but also accelerates training convergence, especially under constrained communication resources.

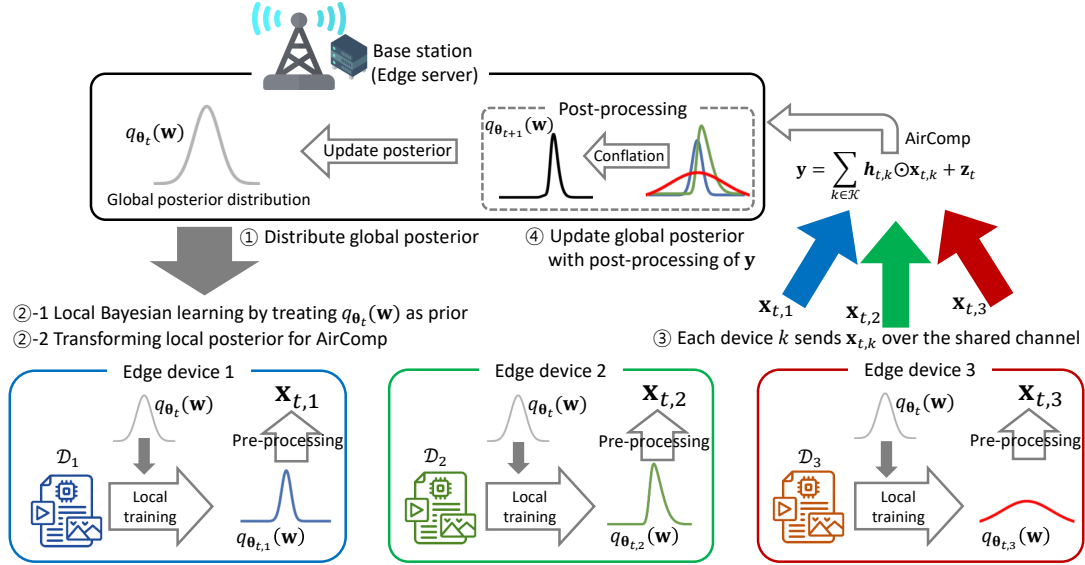


Figure 1. Wireless Bayesian FL with AirComp

III. SYSTEM MODEL

As illustrated in 1, we consider a single cell wireless edge network with K devices distributed in a circular region around a BS, serving as an edge server. We focus on challenging scenarios where the number of participating devices K is large, but each device $k \in \mathcal{K}$ has a small, unbalanced, and non-i.i.d. local dataset \mathcal{D}_k .

The proposed Bayesian FL framework follows the local training and aggregation processes outlined in Subsection II-B, introducing additional mechanisms to address the challenges posed by unstable wireless channels during the delivery of local updates to the server. Communication between each device and the server occurs over random and heterogeneous wireless channels influenced by small-scale fading and path loss. Our framework is centered on designing a transmission method tailored to learning a global variational distribution that effectively represents all distributed local datasets by optimizing the global cost function defined as

$$L(\theta) = \sum_{k \in \mathcal{K}} \pi_k L_k(\theta), \quad (7)$$

where L_k is a local cost function at device $k \in \mathcal{K}$.

A. AirComp under OFDM Fading Channels

To mitigate the excessive resource demands caused by orthogonal channel allocation in large-scale networks, we utilize AirComp approach for local update aggregation. This approach allows devices to concurrently transmit analog-modulated data representing their local posterior distribution updates over a shared channel. By exploiting the superposition property of the wireless medium, the server achieves efficient aggregation of local updates from all devices in constant time, independent of the number of participating devices.

Using the locally optimized variational parameters from (5), each device $k \in \mathcal{K}$ constructs N OFDM symbols to transmit its local update to the BS. Each OFDM symbol $\mathbf{x}_{t,k}^{(n)}$ can

convey up to F analog values over F orthogonal sub-channels, where $n \in \{1, 2, \dots, N\}$. Each OFDM symbol should satisfy the symbol power constraint

$$\|\mathbf{x}_{t,k}^{(n)}\|^2 \leq P. \quad (8)$$

With the power constraint (8), the transmit power of each OFDM symbol cannot exceed P . During the n -th transmission interval, the received signal of BS over F sub-channels are represented by a vector

$$\mathbf{y}_t^{(n)} = \sum_{k \in \mathcal{K}} \mathbf{h}_{t,k} \odot \mathbf{x}_{t,k}^{(n)} + \mathbf{z}_t^{(n)}, \quad (9)$$

where $\mathbf{z}^{(n)} \sim \mathcal{CN}(0, \sigma_z^2 \mathbf{I}_F)$ denotes an effective noise which accounts for additive noise and out-of-cell interference, $\mathbf{h}_{t,k} \in \mathbb{C}^F$ denotes the channel gain vector of device k during the training round t , and the operator \odot denotes the Hadamard product. We consider a Rayleigh block fading channel, where each channel gain remains constant for at least N OFDM symbols and varies independently across training rounds. Specifically, the entries of the channel gain vector are assumed to be i.i.d. complex Gaussian random variables, $\mathbf{h}_{t,k} \sim \mathcal{CN}(0, r_k^{-\alpha} \mathbf{I}_F)$ for $k \in \mathcal{K}$. The channel variance $r_k^{-\alpha}$ accounts for the propagation path-loss from device k to BS, where r_k and α denote the link distance and path-loss exponent, respectively. Since the dissemination of the global Bayesian model and the collection of local updates occur over wireless channels in a time-division duplex (TDD) manner, each device is assumed to know its local channel state information (CSI). On the other hand, the BS is assumed not to know the CSI of each individual device due to the inordinate overhead for the global CSI acquisition in large scale networks.

Note that since local update aggregation in Bayesian FL (6) is not simply an averaging operation as it is in conventional FL, typical AirComp approaches, which aim to directly average local parameters or updates, cannot be applied to update the

global posterior distribution. Furthermore, because channel fading and additive noise introduce estimation errors at the BS, the transmit signal $\mathbf{x}_{t,k}$ should be designed to mitigate the effects of these channel impairments while leveraging the benefits of AirComp to accelerate training convergence.

IV. BAYESIAN FL WITH OVER-THE-AIR POSTERIOR AGGREGATION

A. Gaussian Variational Inference for Local Training

For tractable analysis, we restrict the variational distribution to a Gaussian under the mean-field approximation [10], [23]. Hence, describing the variational posterior distribution explicitly requires twice as many parameters as the model size d . We define the variational parameters $\boldsymbol{\theta} \in \mathbb{R}^{2d}$ as

$$\boldsymbol{\theta} = f(\boldsymbol{\mu}, \boldsymbol{\Sigma}), \quad (10)$$

where $f : \mathbb{R}^{2d} \rightarrow \mathbb{R}^{2d}$ denotes an invertible deterministic function, and $\boldsymbol{\mu} \in \mathbb{R}^d$ and $\boldsymbol{\Sigma} \in \mathbb{R}^{d \times d}$ are respectively the mean vector and diagonal covariance matrix of the model weights $\mathbf{w} \in \mathbb{R}^d$.

Based on Gaussian local and global variational distributions, the computational complexity involved in calculating the KL divergence in (3) can be reduced by applying lemma 1.

Lemma 1. *The KL divergence between two multivariate Gaussian distributions, from $q_1(\mathbf{w}) = \mathcal{N}(\mathbf{w}|\boldsymbol{\mu}_1, \boldsymbol{\Sigma}_1)$ to $q_2(\mathbf{w}) = \mathcal{N}(\mathbf{w}|\boldsymbol{\mu}_2, \boldsymbol{\Sigma}_2)$, has a closed-form expression given by*

$$\begin{aligned} \text{KL}[q_1||q_2] = \frac{1}{2} \left(\log \frac{|\boldsymbol{\Sigma}_2|}{|\boldsymbol{\Sigma}_1|} - d + \text{tr}[\boldsymbol{\Sigma}_2^{-1}\boldsymbol{\Sigma}_1] \right. \\ \left. + (\boldsymbol{\mu}_2 - \boldsymbol{\mu}_1)^\top \boldsymbol{\Sigma}_2^{-1}(\boldsymbol{\mu}_2 - \boldsymbol{\mu}_1) \right). \quad (11) \end{aligned}$$

Proof.

$$\begin{aligned} \text{KL}[q_1||q_2] &= \mathbb{E}_{q_1} \left[\frac{1}{2} \log \frac{|\boldsymbol{\Sigma}_2|}{|\boldsymbol{\Sigma}_1|} + \frac{1}{2} (\mathbf{w} - \boldsymbol{\mu}_2)^\top \boldsymbol{\Sigma}_2^{-1} (\mathbf{w} - \boldsymbol{\mu}_2) \right. \\ &\quad \left. - \frac{1}{2} (\mathbf{w} - \boldsymbol{\mu}_1)^\top \boldsymbol{\Sigma}_1^{-1} (\mathbf{w} - \boldsymbol{\mu}_1) \right] \\ &= \frac{1}{2} \log \frac{|\boldsymbol{\Sigma}_2|}{|\boldsymbol{\Sigma}_1|} + \frac{1}{2} \mathbb{E}_{q_1} \left[(\mathbf{w} - \boldsymbol{\mu}_2)^\top \boldsymbol{\Sigma}_2^{-1} (\mathbf{w} - \boldsymbol{\mu}_2) \right] \\ &\quad - \frac{1}{2} \text{tr} \left[\mathbb{E}_{q_1} [(\mathbf{w} - \boldsymbol{\mu}_1)(\mathbf{w} - \boldsymbol{\mu}_1)^\top] \boldsymbol{\Sigma}_1^{-1} \right] \\ &= \frac{1}{2} \left(\log \frac{|\boldsymbol{\Sigma}_2|}{|\boldsymbol{\Sigma}_1|} + \text{tr}[\boldsymbol{\Sigma}_2^{-1}\boldsymbol{\Sigma}_1] + (\boldsymbol{\mu}_1 - \boldsymbol{\mu}_2)^\top \boldsymbol{\Sigma}_2^{-1} (\boldsymbol{\mu}_1 - \boldsymbol{\mu}_2) - \text{tr}[\mathbf{I}_d] \right) \\ &= \frac{1}{2} \left(\log \frac{|\boldsymbol{\Sigma}_2|}{|\boldsymbol{\Sigma}_1|} + \text{tr}[\boldsymbol{\Sigma}_2^{-1}\boldsymbol{\Sigma}_1] + (\boldsymbol{\mu}_2 - \boldsymbol{\mu}_1)^\top \boldsymbol{\Sigma}_2^{-1} (\boldsymbol{\mu}_2 - \boldsymbol{\mu}_1) - d \right). \quad (12) \end{aligned}$$

□

We define the closed-form expression of the first term in (2) as a regularization loss

$$\begin{aligned} L_{\text{reg},t}(\boldsymbol{\theta}) &= \text{KL}[q_{\boldsymbol{\theta}}(\mathbf{w})||q_{\boldsymbol{\theta}_t}(\mathbf{w})] \\ &= \frac{1}{2} \left(\log \frac{|\boldsymbol{\Sigma}_t|}{|\boldsymbol{\Sigma}|} + \text{tr}[\boldsymbol{\Sigma}_t^{-1}\boldsymbol{\Sigma}] + (\boldsymbol{\mu}_t - \boldsymbol{\mu})^\top \boldsymbol{\Sigma}_t^{-1} (\boldsymbol{\mu}_t - \boldsymbol{\mu}) - d \right). \quad (13) \end{aligned}$$

To address the computational challenges associated with evaluating the second expectation term in (2), we introduce a task loss function that approximates this term using Monte Carlo (MC) sampling

$$L_{\text{task},k}(\boldsymbol{\theta}) = \frac{1}{M} \sum_{m=1}^M -\log p(\mathcal{D}_k|\mathbf{w}_{(m)}), \quad (14)$$

where $\mathbf{w}_{(m)}$ denotes the m -th MC sample drawn from the variational distribution $q_{\boldsymbol{\theta}}(\mathbf{w})$, and M denotes the number of MC samplings. Accordingly, in training round t , each device $k \in \mathcal{K}$ derives the optimized variational posterior distribution by employing the SGD algorithm on the local cost function

$$L_k(\boldsymbol{\theta}) = L_{\text{task},k}(\boldsymbol{\theta}) + \lambda L_{\text{reg},t}(\boldsymbol{\theta}), \quad (15)$$

where λ denotes a positive constant that regulates the degree of deviation from the global posterior distribution during local training.

Eventually, local training aims to derive the local variational parameters $\boldsymbol{\theta}_{t,k}$, which minimize the local cost function (15) for a given dataset \mathcal{D}_k . The local variational distribution is given by

$$q_{\boldsymbol{\theta}_{t,k}}(\mathbf{w}) = \mathcal{N}(\mathbf{w}|\boldsymbol{\mu}_{t,k}, \boldsymbol{\Sigma}_{t,k}), \quad (16)$$

where $\boldsymbol{\mu}_{t,k} \in \mathbb{R}^d$ and $\boldsymbol{\Sigma}_{t,k} \in \mathbb{R}^{d \times d}$ are respectively the mean vector and the diagonal covariance matrix obtained from local training, and $\boldsymbol{\theta}_{t,k} = f(\boldsymbol{\mu}_{t,k}, \boldsymbol{\Sigma}_{t,k})$.

B. AirComp for Posterior Aggregation

Given that the product of Gaussian distributions yields a Gaussian-shaped distribution, the conflated global variational distribution also takes the form of a Gaussian distribution. From (6) and $\{(\boldsymbol{\mu}_{t,k}, \boldsymbol{\Sigma}_{t,k})\}_{k \in \mathcal{K}}$, the global variational distribution is given by

$$\begin{aligned} q_{\boldsymbol{\theta}_{t+1}}(\mathbf{w}) &= C \prod_{k \in \mathcal{K}} \mathcal{N}(\mathbf{w}|\boldsymbol{\mu}_{t,k}, \boldsymbol{\Sigma}_{t,k})^{\pi_k} \\ &= \mathcal{N}(\mathbf{w}|\boldsymbol{\mu}_{t+1}, \boldsymbol{\Sigma}_{t+1}), \quad (17) \end{aligned}$$

where $\boldsymbol{\theta}_{t+1} = f(\boldsymbol{\mu}_{t+1}, \boldsymbol{\Sigma}_{t+1})$, and mean and diagonal covariance matrix are characterized with

$$\boldsymbol{\Sigma}_{t+1}^{-1} = \sum_{k \in \mathcal{K}} \pi_k \boldsymbol{\Sigma}_{t,k}^{-1} \quad (18)$$

$$\boldsymbol{\mu}_{t+1} = \boldsymbol{\Sigma}_{t+1} \sum_{k \in \mathcal{K}} \pi_k \boldsymbol{\mu}_{t,k} \boldsymbol{\Sigma}_{t,k}^{-1}. \quad (19)$$

From the relationship between local and global variational distributions presented in (18) and (19), we observe that aggregating the variational distribution involves summation across devices. Consequently, with some appropriate pre- and post-processing, AirComp can be leveraged to reduce the communication resources required for aggregation in Bayesian FL.

Motivated by this observation, we propose a two-phase FL framework, in which the first phase updates the diagonal covariance matrix and the second phase updates the mean vector of the global variational distribution. Based on (18) and

(19), we define variational parameters for device k at training round t as

$$\boldsymbol{\theta}_{t,k} = \begin{bmatrix} \boldsymbol{\rho}_{t,k} \\ \boldsymbol{\nu}_{t,k} \end{bmatrix}, \quad (20)$$

where

$$\boldsymbol{\rho}_{t,k} = \text{diag}(\boldsymbol{\Sigma}_{t,k}^{-1}), \quad (21)$$

$$\boldsymbol{\nu}_{t,k} = \boldsymbol{\Sigma}_{t+1}^{-1} \boldsymbol{\Sigma}_{t,k}^{-1} \boldsymbol{\mu}_t. \quad (22)$$

Specifically, at the beginning of the first phase, a new variational parameter vector $\boldsymbol{\rho}_{t,k}$ is defined for each device $k \in \mathcal{K}$, initialized as

$$\boldsymbol{\rho}_{t,k} \leftarrow \text{diag}(\boldsymbol{\Sigma}_t^{-1}). \quad (23)$$

By applying the reparameterization trick with (23), each device k generates MC samples from $\mathcal{N}(\boldsymbol{\mu}_t, \boldsymbol{\Sigma}_{t,k})$ according to

$$\mathbf{w}^{(m)} = \boldsymbol{\rho}_{t,k}^{-\frac{1}{2}} \odot \boldsymbol{\epsilon}^{(m)} + \boldsymbol{\mu}_t, \quad (24)$$

where $\boldsymbol{\epsilon}^{(m)} \in \mathbb{R}^d$ is the m -th MC sample from $\mathcal{N}(0, \mathbf{I}_d)$, and $\boldsymbol{\rho}_{t,k}^{-\frac{1}{2}}$ is the element-wise inverse square root of $\boldsymbol{\rho}_{t,k}$. The local cost function $L_k(\boldsymbol{\mu}_t, \boldsymbol{\rho}_{t,k})$ is computed using M independent MC samples, and a gradient descent step for the variational parameter vector $\boldsymbol{\rho}_{t,k}$ is given by

$$\boldsymbol{\rho}_{t,k} \leftarrow \boldsymbol{\rho}_{t,k} - \eta \nabla_{\boldsymbol{\rho}} L_k(\boldsymbol{\mu}_t, \boldsymbol{\rho}_{t,k}). \quad (25)$$

The local update of $\boldsymbol{\rho}_{t,k}$ is performed over E gradient descent steps.

After the local training, the local update vector of $\boldsymbol{\rho}_{t,k}$ is represented as

$$\boldsymbol{\Delta}_{\rho_{t,k}} = \boldsymbol{\rho}_{t,k} - \boldsymbol{\rho}_t. \quad (26)$$

The update vector $\boldsymbol{\Delta}_{\rho_{t,k}}$ is partitioned into N_1 groups based on a predefined grouping rule. Then, the update values in each group is transmitted over F sub-channels of an OFDM symbol, represented by the vector $\boldsymbol{\Delta}_{\rho_{t,k}}^{(n_1)} \in \mathbb{R}^F$ for OFDM symbol $n_1 \in \{1, 2, \dots, N_1\}$. To accommodate cases where the number of values in a group is less than F , zeros are padded, ensuring that $\boldsymbol{\Delta}_{\rho_{t,k}}^{(n_1)}$ forms a F -dimensional vector.

In AirComp transmissions, it is crucial for each device to carefully control its transmit power to ensure that the received signal strengths at the BS are aligned, even under varying channel fading conditions across devices. To achieve this, the BS first calculates the average update power $\bar{\delta}_{\rho_t}$ by collecting the local update powers $\frac{1}{d} \|\boldsymbol{\Delta}_{\rho_{t,k}}\|^2$ from all devices and then computing their weighted average as follows

$$\bar{\delta}_{\rho_t} = \sum_{k \in \mathcal{K}} \frac{\pi_k}{d} \|\boldsymbol{\Delta}_{\rho_{t,k}}\|^2. \quad (27)$$

The BS then sends $\bar{\delta}_{\rho_t}$ back to all devices. We assume these magnitudes are delivered without errors and require only negligible communication resources, since each is a single scalar value. Using (27) and local channel state information,

each device k then computes its power allocation vectors $\mathbf{p}_{t,k}^{(n_1)} \in \mathbb{R}^F$ for symbols $n_1 \in \{1, 2, \dots, N_1\}$ according to

$$\begin{aligned} \mathbf{p}_{t,k}^{(n_1)} &= \pi_k^2 \gamma \mathbf{g}_{t,k} \odot \frac{\mathbf{v}_{\rho_{t,k}}^{(n_1)} \odot \mathbf{v}_{\rho_{t,k}}^{(n_1)}}{\bar{\delta}_{\rho_t}} \\ &= \mathbf{u}_{t,k} \odot \left(\mathbf{v}_{\rho_{t,k}}^{(n_1)} \odot \mathbf{v}_{\rho_{t,k}}^{(n_1)} \right), \end{aligned} \quad (28)$$

where γ denotes a positive coefficient for power scaling, $\mathbf{g}_{t,k} \in \mathbb{R}^F$ denotes the channel power inversion whose entry $f \in \{1, 2, \dots, F\}$ is defined as $g_{t,k,f} = |h_{t,k,f}|^{-2}$, and $\mathbf{v}_{\rho_{t,k}}^{(n_1)} \in \mathbb{R}^F$ denotes a power control vector to be optimized. The vector $\mathbf{u}_{t,k} = \frac{\pi_k^2 \gamma}{\bar{\delta}_{\rho_{t,k}}} \mathbf{g}_{t,k}$ helps to preserve a certain level of received SNR under channel fading, while $\mathbf{v}_{\rho_{t,k}}^{(n_1)}$ constrains the magnitudes of the entries in $\boldsymbol{\Delta}_{\rho_{t,k}}^{(n_1)}$ to satisfy the power constraint (8), $\|\mathbf{p}_{t,k}^{(n_1)}\|_1 \leq P$. Eventually, each device $k \in \mathcal{K}$ reports the power-constrained version of local update vector $\text{sgn}(\boldsymbol{\Delta}_{\rho_{t,k}}^{(n_1)}) \odot \mathbf{v}_{\rho_{t,k}}^{(n_1)}$ instead of $\boldsymbol{\Delta}_{\rho_{t,k}}^{(n_1)}$, where $\text{sgn}(\cdot)$ denotes the element-wise signum function. In the training round t , the device k constitutes n_1 -th symbol as

$$\mathbf{x}_{t,k}^{(n_1)} = \text{sgn}(\mathbf{h}_{t,k})^* \odot \text{sgn}(\boldsymbol{\Delta}_{\rho_{t,k}}^{(n_1)}) \odot \sqrt{\mathbf{p}_{t,k}^{(n_1)}}, \quad (29)$$

where $\sqrt{\cdot}$ denotes the entry-wise square root function.

With the synchronized transmissions of $\mathbf{x}_{t,k}^{(n_1)}$ from all devices $k \in \mathcal{K}$ over the shared channels, the received signal (9) can be rewritten as

$$\mathbf{y}_t^{(n_1)} = \sum_{k \in \mathcal{K}} \pi_k \sqrt{\frac{\gamma}{\bar{\delta}_{\rho_{t,k}}}} \text{sgn}(\boldsymbol{\Delta}_{\rho_{t,k}}^{(n_1)}) \odot \mathbf{v}_{\rho_{t,k}}^{(n_1)} + \mathbf{z}_t^{(n_1)}, \quad (30)$$

where $\mathbf{z}_t^{(n_1)} \sim \mathcal{CN}(0, \sigma_z^2 \mathbf{I}_F)$. Then, the aggregated update vector is estimated as

$$\begin{aligned} \hat{\boldsymbol{\Delta}}_{\rho_t}^{(n_1)} &= \sqrt{\frac{\bar{\delta}_{\rho_t}}{\gamma}} \mathbf{y}_t^{(n_1)} \\ &= \left(\sum_{k \in \mathcal{K}} \pi_k \boldsymbol{\Delta}_{\rho_{t,k}}^{(n_1)} \right) + \eta \boldsymbol{\xi}_{\rho_t}^{(n_1)} + \sqrt{\frac{\bar{\delta}_{\rho_{t,k}}}{\gamma}} \mathbf{z}_t^{(n_1)}, \end{aligned} \quad (31)$$

where $\boldsymbol{\xi}_{\rho_t}^{(n_1)} = \sum_{k \in \mathcal{K}} \pi_k \text{sgn}(\boldsymbol{\Delta}_{\rho_{t,k}}^{(n_1)}) \odot \mathbf{e}_{\rho_{t,k}}^{(n_1)}$ denotes the aggregated update error, and $\mathbf{e}_{\rho_{t,k}}^{(n_1)} = \frac{1}{\eta} (\mathbf{v}_{\rho_{t,k}}^{(n_1)} - |\boldsymbol{\Delta}_{\rho_{t,k}}^{(n_1)}|)$ denotes the local update error resulting from power-constrained transmissions of device k . By re-arranging the values of the vectors (31) for all $n \in \{1, 2, \dots, N_1\}$ according to a predefined reverse grouping rule, the BS constitutes the aggregated composite update vector $\hat{\boldsymbol{\Delta}}_{\rho_t} \in \mathbb{R}^d$. Based on the composite update vector, the BS updates the variational parameters associated with the covariance matrix of the global variational posterior as

$$\boldsymbol{\rho}_{t+1} = \boldsymbol{\rho}_t + \hat{\boldsymbol{\Delta}}_{\rho_t}. \quad (32)$$

Then, the BS distributes the updated global covariance matrix $\boldsymbol{\Sigma}_{t+1} = \text{diag}(\boldsymbol{\rho}_{t+1})^{-1}$ to all devices.

In the second phase, for each device $k \in \mathcal{K}$, a new variational parameter vector $\boldsymbol{\nu}_{t,k}$ is defined using the received covariance matrix $\boldsymbol{\Sigma}_{t+1}$ and it is initialized as

$$\boldsymbol{\nu}_{t,k} \leftarrow \boldsymbol{\Sigma}_{t,k}^{-1} \boldsymbol{\Sigma}_{t+1} \boldsymbol{\mu}_t. \quad (33)$$

Using the reparameterization trick and (33), each device k generates MC samples from $\mathcal{N}(\boldsymbol{\mu}_{t,k}, \boldsymbol{\Sigma}_{t+1})$ as

$$\boldsymbol{\theta} = \boldsymbol{\Sigma}_{t+1}^{\frac{1}{2}} \boldsymbol{\epsilon} + \boldsymbol{\Sigma}_{t+1}^{-1} \boldsymbol{\Sigma}_{t,k} \boldsymbol{\nu}_{t,k}. \quad (34)$$

Similarly to (25), the local variational parameter vector $\boldsymbol{\nu}_{t,k}$ is updated at each gradient descent step as

$$\boldsymbol{\nu}_{t,k} \leftarrow \boldsymbol{\nu}_{t,k} - \eta \nabla_{\boldsymbol{\nu}} L_k(\boldsymbol{\nu}_{t,k}, \text{diag}(\boldsymbol{\Sigma}_{t+1}^{-1})). \quad (35)$$

After completing E gradient descent steps, each device forms its local update vector $\boldsymbol{\Delta}_{\nu_{t,k}} = \boldsymbol{\nu}_{t,k} - \boldsymbol{\nu}_t$ and obtains the average update power $\bar{\delta}_{\nu_t}$ using the similar procedures described in (26) and (27), respectively. It then partitions $\boldsymbol{\Delta}_{\nu_{t,k}}$ into N_2 groups and transmits the update values in each group via OFDM symbols $n_2 \in \{N_1 + 1, N_1 + 2, \dots, N_1 + N_2\}$ according to the similar procedures described in (28) and (29). The BS estimates the aggregated update vector in a similar manner to (30). Then, the aggregated update vector for $\boldsymbol{\nu}_t$ is given by

$$\begin{aligned} \hat{\boldsymbol{\Delta}}_{\nu_t}^{(n_2)} &= \sqrt{\frac{\bar{\delta}_{\nu_{t,k}}}{\gamma}} \mathbf{y}_t^{(n_2)} \\ &= \left(\sum_{k \in \mathcal{K}} \pi_k \boldsymbol{\Delta}_{\nu_{t,k}}^{(n_2)} \right) + \eta \boldsymbol{\xi}_{\nu_t}^{(n_2)} + \sqrt{\frac{\bar{\delta}_{\nu_{t,k}}}{\gamma}} \mathbf{z}_t^{(n_2)}, \end{aligned} \quad (36)$$

where $\mathbf{z}_t^{(n_2)} \sim \mathcal{CN}(0, \sigma_z^2 \mathbf{I}_F)$, $\boldsymbol{\xi}_{\nu_t}^{(n_2)} = \sum_{k \in \mathcal{K}} \pi_k \text{sgn}(\boldsymbol{\Delta}_{\nu_{t,k}}^{(n_2)}) \odot \mathbf{e}_{\nu_{t,k}}^{(n_2)}$, and $\mathbf{e}_{\nu_{t,k}}^{(n_2)} = \frac{1}{\eta} (\mathbf{v}_{\nu_{t,k}}^{(n_2)} - |\boldsymbol{\Delta}_{\nu_{t,k}}^{(n_2)}|)$. The BS reconstructs the complete update vector $\hat{\boldsymbol{\Delta}}_{\nu_t}$ by re-arranging the update values delivered via N_2 OFDM symbols and updates the variational parameter vector as

$$\boldsymbol{\nu}_{t+1} = \boldsymbol{\nu}_t + \hat{\boldsymbol{\Delta}}_{\nu_t}. \quad (37)$$

Note that $\boldsymbol{\nu}_{t+1}$ is identical to $\boldsymbol{\mu}_{t+1}$ according to (19). The BS then proceeds to the next training round $t + 1$ by distributing the updated global mean vector $\boldsymbol{\mu}_{t+1}$ to all devices if the convergence condition is not satisfied.

V. CONVERGENCE ANALYSIS AND TRANSMIT POWER CONTROL

In this section, we analyze the convergence of our proposed framework under given power allocations and investigate the impact of fading channels and limited power budget on the training convergence rate. Subsequently, leveraging these observations, we optimize the transmit power allocation to enhance the training convergence.

A. Convergence Analysis

For applications to deep neural networks, we investigate the convergence to stationary points, without assuming the convexity.

Algorithm 1 Bayesian FL with Over-the-Air Posterior Aggregation

```

1: Initialize:
    $t \leftarrow 0$ 
    $\boldsymbol{\mu}_t, \boldsymbol{\Sigma}_t \leftarrow$  Random initialization
2: BS distributes  $\boldsymbol{\mu}_0$  and  $\boldsymbol{\Sigma}_0$  to all devices
3: while convergence criterion is not met do
   // Phase 1: Update global covariance matrix
4:   for each device  $k \in \mathcal{K}$  in parallel do
5:      $\boldsymbol{\rho}_{t,k} \leftarrow \text{diag}(\boldsymbol{\Sigma}_t^{-1})$ 
6:     for  $i = 1$  to  $E$  do
7:        $\boldsymbol{\rho}_{t,k} \leftarrow \boldsymbol{\rho}_{t,k} - \eta \nabla_{\boldsymbol{\rho}} L_k(\boldsymbol{\mu}_t, \boldsymbol{\rho}_{t,k})$ 
8:     end for
9:     Compute  $\boldsymbol{\Delta}_{\rho_{t,k}}$  with (26)
10:    Optimize power allocation  $\{\mathbf{p}_{t,k}^{(n_1)}\}_{n_1=1}^{N_1}$ 
11:    Form  $\{\mathbf{x}_{t,k}^{(n_1)}\}_{n_1=1}^{N_1}$  with (29) and transmit them
12:  end for
13:  BS reconstructs  $\hat{\boldsymbol{\Delta}}_{\rho_t}$  from  $\{\mathbf{y}_t^{(n_1)}\}_{n_1=1}^{N_1}$  with (31)
14:   $\boldsymbol{\rho}_{t+1} = \boldsymbol{\rho}_t + \bar{\delta}_{\rho_t} \hat{\boldsymbol{\Delta}}_{\rho_t}$ 
15:  BS distributes  $\boldsymbol{\Sigma}_{t+1} = \text{diag}(\boldsymbol{\rho}_{t+1})^{-1}$  to all devices
   // Phase 2: Update global mean vector
16:  for each device  $k \in \mathcal{K}$  in parallel do
17:     $\boldsymbol{\nu}_{t,k} \leftarrow \boldsymbol{\Sigma}_{t,k}^{-1} \boldsymbol{\Sigma}_{t+1} \boldsymbol{\mu}_t$ 
18:    for  $i = 1$  to  $E$  do
19:       $\boldsymbol{\nu}_{t,k} \leftarrow \boldsymbol{\nu}_{t,k} - \eta \nabla_{\boldsymbol{\nu}} L_k(\boldsymbol{\nu}_{t,k}, \text{diag}(\boldsymbol{\Sigma}_{t+1}^{-1}))$ 
20:    end for
21:    Compute the normalized update vector  $\boldsymbol{\Delta}_{\nu_{t,k}}$ 
22:    Optimize power allocation  $\{\mathbf{p}_{t,k}^{(n_2)}\}_{n_2=N_1+1}^{N_1+N_2}$ 
23:    Form  $\{\mathbf{x}_{t,k}^{(n_2)}\}_{n_2=1}^{N_1+N_2}$  and transmit them
24:  end for
25:  BS reconstructs  $\hat{\boldsymbol{\Delta}}_{\nu_t}$  from  $\{\mathbf{y}_t^{(n_2)}\}_{n_2=N_1+1}^{N_1+N_2}$ 
26:   $\boldsymbol{\nu}_{t+1} = \boldsymbol{\nu}_t + \bar{\delta}_{\nu_t} \hat{\boldsymbol{\Delta}}_{\nu_t}$ 
27:  BS distributes  $\boldsymbol{\mu}_{t+1} = \boldsymbol{\nu}_{t+1}$  to all devices
28:   $t \leftarrow t + 1$ 
29: end while

```

Assumption 1 (Smooth). For any $\boldsymbol{\nu}_1, \boldsymbol{\nu}_2, \boldsymbol{\rho}_1, \boldsymbol{\rho}_2 \in \mathbb{R}^d$, the global loss function $L(\boldsymbol{\nu}, \boldsymbol{\rho})$ is assumed to satisfy

$$\begin{aligned} & |L(\boldsymbol{\nu}_1, \boldsymbol{\rho}) - L(\boldsymbol{\nu}_2, \boldsymbol{\rho}) - \nabla_{\boldsymbol{\nu}} L(\boldsymbol{\nu}_2, \boldsymbol{\rho})^\top (\boldsymbol{\nu}_1 - \boldsymbol{\nu}_2)| \\ & \leq \frac{\Lambda_{\nu}}{2} \|\boldsymbol{\nu}_1 - \boldsymbol{\nu}_2\|^2 \end{aligned} \quad (38)$$

$$\begin{aligned} & |L(\boldsymbol{\nu}, \boldsymbol{\rho}_1) - L(\boldsymbol{\nu}, \boldsymbol{\rho}_2) - \nabla_{\boldsymbol{\rho}} L(\boldsymbol{\nu}, \boldsymbol{\rho}_2)^\top (\boldsymbol{\rho}_1 - \boldsymbol{\rho}_2)| \\ & \leq \frac{\Lambda_{\rho}}{2} \|\boldsymbol{\rho}_1 - \boldsymbol{\rho}_2\|^2 \end{aligned} \quad (39)$$

for non-negative constants Λ_{ν} and Λ_{ρ} .

For simplicity, we assume $d = F$ and a single epoch $E = 1$ for local training in the subsequent convergence analysis. Consequently, the number of transmissions in each phase becomes $N_1 = N_2 = 1$, and the local updates simplify to $\boldsymbol{\Delta}_{\rho_{t,k}} = -\eta \nabla_{\boldsymbol{\rho}} L_k(\boldsymbol{\mu}_t, \boldsymbol{\rho}_t)$ and $\boldsymbol{\Delta}_{\nu_{t,k}} = -\eta \nabla_{\boldsymbol{\nu}} L_k(\boldsymbol{\nu}_{t,k}, \text{diag}(\boldsymbol{\Sigma}_{t+1}^{-1}))$.

Theorem 1. Under Assumption 1, with the learning rate set as $\eta = \frac{1}{\sqrt{T}}$, the expected decrease in the cost function over T training rounds is lower bounded by (40).

$$\begin{aligned}
\mathbb{E}[L(\boldsymbol{\nu}_0, \boldsymbol{\rho}_0) - L(\boldsymbol{\nu}_T, \boldsymbol{\rho}_T)] &\geq \frac{1}{2\sqrt{T}} \mathbb{E} \left[\sum_{t=0}^{T-1} \left(1 - \frac{\Lambda_\rho}{\sqrt{T}} \right) \|\nabla_\rho L(\boldsymbol{\mu}_t, \boldsymbol{\rho}_t)\|^2 + \left(1 - \frac{\Lambda_\nu}{\sqrt{T}} \right) \|\nabla_\nu L(\boldsymbol{\nu}_t, \text{diag}(\boldsymbol{\Sigma}_{t+1}^{-1}))\|^2 \right] \\
&\quad - \underbrace{\frac{\sigma_z^2}{2\gamma T} \mathbb{E} \left[\sum_{t=0}^{T-1} \sum_{k \in \mathcal{K}} \pi_k \left(\Lambda_\rho \|\nabla_\rho L_k(\boldsymbol{\mu}_t, \boldsymbol{\rho}_{t,k})\|^2 + \Lambda_\nu \|\nabla_\nu L_k(\boldsymbol{\nu}_{t,k}, \text{diag}(\boldsymbol{\Sigma}_{t+1}^{-1}))\|^2 \right) \right]}_{\text{Channel noise}} \\
&\quad - \underbrace{\frac{1}{2\sqrt{T}} \mathbb{E} \left[\sum_{t=0}^{T-1} \left(1 + \frac{\Lambda_\rho}{\sqrt{T}} \right) \|\boldsymbol{\xi}_{\rho_t}\|^2 + \left(1 + \frac{\Lambda_\nu}{\sqrt{T}} \right) \|\boldsymbol{\xi}_{\nu_t}\|^2 \right]}_{\text{Limited transmission power budget}}
\end{aligned} \tag{40}$$

Proof. Refer to Appendix A. \square

As shown in Theorem 1, channel noise and update errors, $\boldsymbol{\xi}_{\rho_t}$ and $\boldsymbol{\xi}_{\nu_t}$, caused by the limited transmission power budget pose obstacles to minimizing the cost function and, consequently, to advancing model training. Note that update errors are highly dependent on channel conditions. Specifically, as shown in (28), when the entries of the channel power inversion vector $\mathbf{g}_{t,k}$ are large, the update magnitude vector, $\mathbf{v}_{\rho_{t,k}}$ or $\mathbf{v}_{\nu_{t,k}}$, must be reduced to meet the power constraint, leading to increased update errors.

Corollary 1. *In the asymptotic regime as $T \rightarrow \infty$, the round-averaged squared ℓ_2 norm of the global update vectors is upper-bounded by*

$$\begin{aligned}
&\mathbb{E} \left[\frac{1}{T} \sum_{t=0}^{T-1} \|\nabla_\rho L(\boldsymbol{\mu}_t, \boldsymbol{\rho}_t)\|^2 + \|\nabla_\nu L(\boldsymbol{\nu}_t, \text{diag}(\boldsymbol{\Sigma}_{t+1}^{-1}))\|^2 \right] \\
&\leq \mathbb{E} \left[\frac{1}{T} \sum_{t=0}^{T-1} \|\boldsymbol{\xi}_{\rho_t}\|^2 + \|\boldsymbol{\xi}_{\nu_t}\|^2 \right] + \frac{1}{\sqrt{T}} (L(\boldsymbol{\nu}_0, \boldsymbol{\rho}_0) - L(\boldsymbol{\nu}^*, \boldsymbol{\rho}^*)),
\end{aligned} \tag{41}$$

where $\boldsymbol{\nu}^*$ and $\boldsymbol{\rho}^*$ denote the optimal variational parameter vectors that minimize the global cost function.

Proof. In the asymptotic regime as $T \rightarrow \infty$, combining Theorem 1 with the inequality $L(\boldsymbol{\nu}_T, \boldsymbol{\rho}_T) \geq L(\boldsymbol{\nu}^*, \boldsymbol{\rho}^*)$ yields (41). \square

The Corollary 1 indicates that the impact of additive noise on convergence becomes negligible after a sufficiently large number of training rounds. Consequently, given a finite initial cost function $L(\boldsymbol{\nu}_0, \boldsymbol{\rho}_0)$, convergence of the proposed framework is guaranteed as long as the average aggregated update errors of the variational parameters vanishes. This implies that the transmit signal should be designed to minimize the aggregated update errors, $\|\boldsymbol{\xi}_{\rho_t}\|^2$ and $\|\boldsymbol{\xi}_{\nu_t}\|^2$, to accelerate the training convergence. Interestingly, although the proposed framework adopts a distinct approach from conventional AirComp-based FL [13]–[15] in terms of local training and update aggregation, it exhibits similar convergence behavior, in that the learning performance is largely influenced by the aggregated update error.

B. Transmit Power Optimization

In the proposed framework, the transmit signal is governed by the update magnitude vector, $\mathbf{v}_{\rho_{t,k}}^{(n_1)}$ or $\mathbf{v}_{\nu_{t,k}}^{(n_2)}$, as defined in (28) and (29). Given that the aggregated update errors from the two variational parameters have an equal impact on training convergence as shown in (41), the same power optimization process is applied to both $\mathbf{v}_{\rho_{t,k}}^{(n_1)}$ and $\mathbf{v}_{\nu_{t,k}}^{(n_2)}$. To avoid redundancy, we focus on the optimization of $\mathbf{v}_{\rho_{t,k}}^{(n_1)}$ in the remainder of this subsection.

As a distributed method to reduce the aggregate error $\|\boldsymbol{\xi}_{\rho_t}\|^2$, each device k optimizes $\mathbf{v}_{\rho_{t,k}}^{(n_1)}$ to minimize its local update error under a given power budget by solving the following optimization problem:

$$\begin{aligned}
&\underset{\mathbf{v} \in \mathbb{R}^F}{\text{minimize}} \quad \|\boldsymbol{\Delta}_{\rho_{t,k}}^{(n_1)} - \mathbf{v}\|^2 \\
&\text{subject to} \quad \mathbf{u}_{t,k}^T (\mathbf{v} \odot \mathbf{v}) \leq P \\
&\quad \quad \quad v_f \geq 0, \quad f = 1, 2, \dots, F
\end{aligned} \tag{42}$$

The power optimization (42) is a quadratically constrained quadratic programming (QCQP) problem, and its solution, derived from the Karush-Kuhn-Tucker (KKT) conditions, is given by

$$\begin{aligned}
&\mathbf{v}_{\rho_{t,k}}^{(n_1)} \\
&= \begin{cases} |\boldsymbol{\Delta}_{\rho_{t,k}}^{(n_1)}|, & \text{if } \mathbf{u}_{t,k}^T (\boldsymbol{\Delta}_{\rho_{t,k}}^{(n_1)} \odot \boldsymbol{\Delta}_{\rho_{t,k}}^{(n_1)}) \leq P \\ |\boldsymbol{\Delta}_{\rho_{t,k}}^{(n_1)}| \odot (\mathbf{1}_F + \lambda_{\rho_{t,k}}^{(n_1)} \mathbf{u}_{t,k}) & \text{Otherwise} \end{cases},
\end{aligned} \tag{43}$$

where the operation \odot denotes the Hadamard (element-wise) division, $\mathbf{1}_F \in \mathbb{R}^F$ is the all-ones vector, and $\lambda_{\rho_{t,k}}^{(n_1)}$ is a scalar satisfying $\mathbf{u}_{\rho_{t,k}}^T (\mathbf{v}_{\rho_{t,k}}^{(n_1)} \odot \mathbf{v}_{\rho_{t,k}}^{(n_1)}) = P$. From the expression of the optimized power control vector in (43), we observe that device k can transmit its local update without reducing the update magnitudes when the updates are small or the elements of $\mathbf{u}_{\rho_{t,k}}$ are low. The latter typically occurs under favorable channel conditions or with a small local dataset. Otherwise, the update magnitude must be scaled down to satisfy the transmit power constraint. In particular, the reduction factor $(1 + \lambda_{\rho_{t,k}}^{(n_1)} u_{t,k,f})$ is inversely proportional to the channel power gain of each sub-channel. For example, a local update value transmitted over sub-channel f must be significantly attenuated if the channel gain of that sub-channel is poor.

It is worth noting that the optimized power control in (43), along with the associated discussion, is also applicable

Table I
SIMULATION ENVIRONMENT

Symbol	Description	Value
r_{cylge}	BS coverage	200 [meters]
K	Number of edge devices	40
$ \mathcal{D}_k $	Device k 's dataset size (data samples from a single label)	Poisson r.v. with mean 10
P	Maximum symbol power	23 [dBm]
σ_z^2	Effective noise power	-74 [dBm]
F	Number of sub-channels	1,024
N_1, N_2	Number of symbol transmissions	$N_1 = N_2 = \lceil d/F \rceil = 61$
α	Path loss exponent	4

Table II
TRAINING HYPER-PARAMETERS

Symbol	Description	Value
η	Learning rate in local training	0.1
B	Mini-batch size in local training	10
E	Local training epoch	3
d	Number of DNN weights	62,346
γ	Coefficient for power scaling	10 [dB]
λ	Weight for KL divergence	1/50,000
M	Number of MC samplings	5

to the AirComp-based aggregation in the second phase by substituting $\Delta_{\rho_t, k}^{(n_1)}$ with $\Delta_{\nu_t, k}^{(n_2)}$.

VI. SIMULATION RESULTS

In this section, through extensive simulations, we demonstrate that the proposed distribution-level AirComp framework can effectively address challenges arising from realistic wireless edge networks, such as data scarcity and heterogeneity. This is substantiated by comparisons with AirComp-based conventional FL methods in terms of channel uses needed for convergence, test accuracy, and calibration performance. All simulation codes were implemented in Python 3.12.7 using NumPy 1.26.4, PyTorch 2.5.1, and the Blitz package [28]. As benchmark methods, we consider several representative FL algorithms designed to address data heterogeneity: FedAvg [1], FedProx [3], and SCAFFOLD [4]. These methods employ a frequentist approach for local training, and we apply the optimized power allocation method developed in [13] for amplitude alignment over wireless networks.

We consider a wireless edge network scenario in which a total of 40 edge devices are uniformly distributed within a 200-meter radius of the BS. For all simulations, the MNIST dataset is employed. Each device possesses data samples from only a single class label, and the number of samples per device is drawn from a Poisson distribution with a mean of 10, resulting in both data scarcity and label skew. Unless otherwise indicated, all experimental results are obtained using the simulation setup and training hyper-parameters summarized in Tables I and II, respectively. Note that the extremely limited and skewed training data in this scenario makes the learning performance highly sensitive to the randomness in both the local dataset size and the assigned label for each device. As a result, even with identical simulation settings described in Tables I and II, the outcomes can vary considerably depending

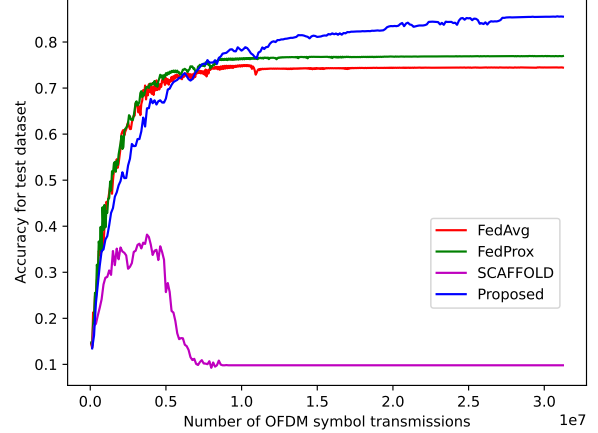


Figure 2. Comparison of wireless FL methods in scenario with scarce and heterogeneous data

on how data is distributed across devices. To account for this effect and ensure a fair performance evaluation, all simulation results are averaged over 10 independent realizations of local dataset sizes and label assignments.

Through FL, we train a three-layer convolutional neural network (CNN) architecture, as adopted in relevant works [13], [15], [16]. The architecture consists of two convolutional layers, each followed by a 2×2 max pooling layer and a ReLU activation function. The first convolutional layer uses 32 filters of size 5×5 , while the second uses 64 filters of size 5×5 . After the convolutional and pooling layers, a fully connected layer with 1,024 units is added, followed by a softmax output layer for classification. For this architecture, the total number of model weights is $d = 62,346$. Note that in this architecture, FedAvg and FedProx each transmit d real values corresponding to the model weights in every training round. SCAFFOLD and the proposed framework, on the other hand, transmit $2d$ real values per round. For SCAFFOLD, these consist of d values for the model weights and d values for the control variate, which serves to mitigate client drift. In the proposed framework, the $2d$ values represent the mean and variance parameters of the variational posterior distributions for the weights.

A. Convergence Speed and Final Test Accuracy

In this subsection, we present simulation results on the test accuracy of FL methods with respect to the number of channel uses for local update aggregation in diverse environments. These results allow us to assess both the convergence speed and the test accuracy upon convergence, as well as to understand the effect of system parameters on training performance.

Figure 2 presents the training progress of the proposed framework and benchmark FL methods as a function of the number of channel uses required for update aggregation. The proposed framework demonstrates higher test accuracy compared to the benchmark methods. This improvement is achieved by mitigating local overfitting and client drift through

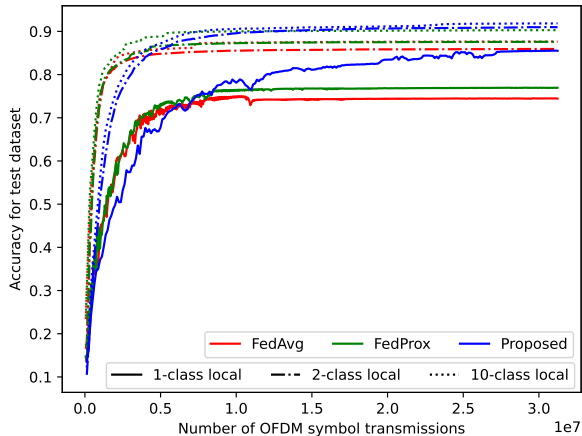


Figure 3. Training progress under different degrees of local label skewness

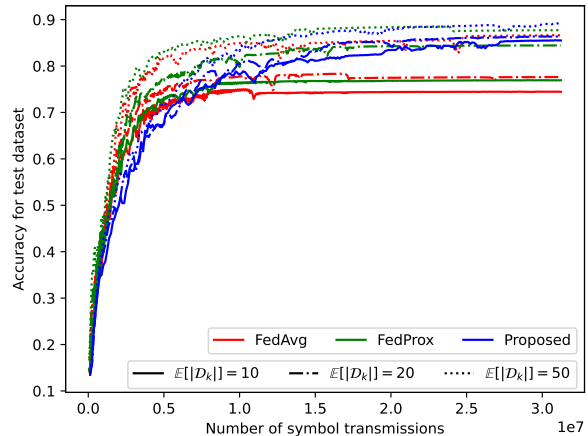


Figure 4. Training progress for different local dataset sizes

Bayesian local training and distribution-level aggregation. Even though the proposed framework requires twice as many channel uses as FedAvg and FedProx in each training round, it does not significantly delay the convergence in the initial rounds. This is because its distribution-level aggregation allows the BS to more effectively update the global model by accounting for model uncertainty during the aggregation of local training results. FedProx is shown to provide a performance gain over FedAvg; however, this improvement is limited in our scenario characterized by extremely scarce and heterogeneous data. Furthermore, SCAFFOLD is prone to collapse due to its high sensitivity to noise in the control variate. For this reason, it is not well-suited to analog AirComp environments where noisy signal recovery is unavoidable; therefore, SCAFFOLD is excluded from the following simulation results.

Figure 3 illustrates the training progress of the proposed framework and benchmark methods across varying degrees of label skewness. As the label skewness decreases, all methods generally exhibit improved training performance due to mitigated client drift and reduced local overfitting. Interestingly, the proposed framework consistently demonstrates significant performance gains over the benchmark methods across all skewness levels, particularly in terms of the test accuracy of the converged model. Furthermore, the proposed method shows relatively low sensitivity to changes in skewness, indicating that the distribution-level aggregation used in our framework effectively addresses the inherent challenges posed by data heterogeneity. Conversely, FedProx provides only marginal improvements over FedAvg regardless of the degree of skewness, implying limited effectiveness of its regularization approach in scenarios characterized by data scarcity.

Figure 4 illustrates the training progress of the proposed framework and benchmark methods across varying local dataset sizes. As the local dataset size increases, the training performance of all methods improves due to the reduced variance of locally trained models. Consistent with the observations from Figure 3, the proposed framework achieves the highest test accuracy in the converged model and exhibits the

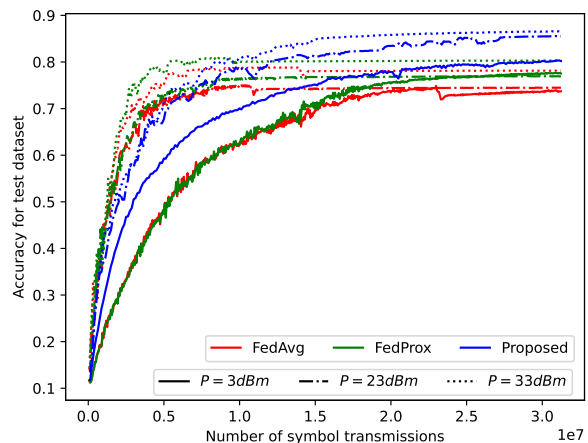


Figure 5. Training progress for different transmission power budgets

smallest performance variation across different local dataset sizes. This demonstrates the robustness of the proposed framework against the challenges arising from limited local data.

Figure 5 illustrates the training progress of the proposed framework and benchmark methods under varying transmission power budgets at the edge devices. As the transmission power budget increases, all methods exhibit improved training performance, primarily due to the reduction in update errors caused by limited transmission power. In particular, as established in the convergence analysis, the decrease in update error with higher power budgets leads to faster convergence of the proposed framework. Consistent with previous results, the proposed framework achieves the highest test accuracy upon convergence across all power budget levels, demonstrating its robustness to power limitations. These observations highlight the importance of sufficient transmission power in accelerating model convergence in wireless federated learning.

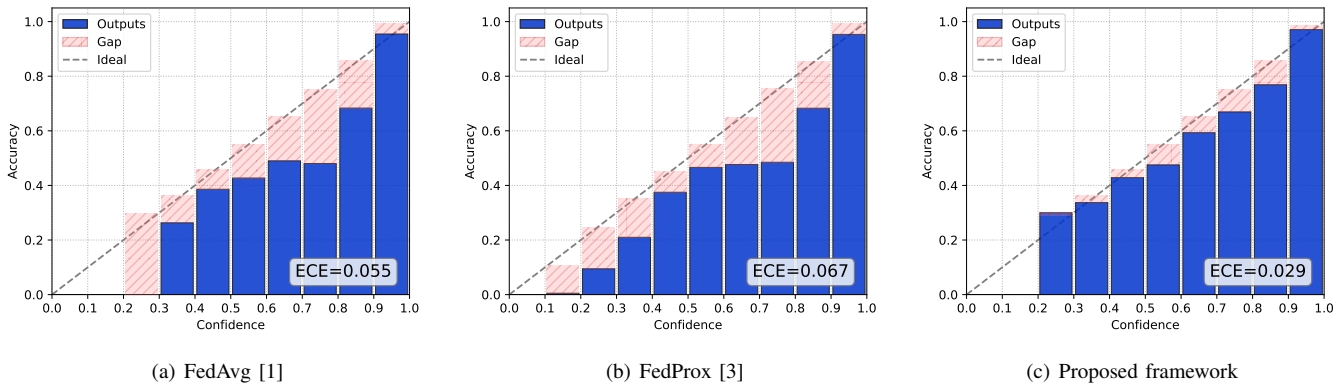


Figure 6. Comparison of reliability diagrams for different FL methods

B. Calibration Performance

In scenarios where inference performance is constrained by scarce and heterogeneous data, calibration performance plays a critical role in ensuring the reliability of model predictions. This aspect is particularly important for safety-critical applications. In other words, the predicted probabilities produced by the model should be trustworthy and should accurately reflect the true likelihood of each outcome. For example, in the classification of MNIST data, the model’s confidence score, which is typically represented by the largest softmax output, should correspond closely to the actual accuracy observed for samples assigned that level of confidence. In this subsection, we evaluate the calibration performance of various FL methods by presenting both reliability diagrams and the expected calibration error (ECE) [29].

The reliability diagram visualizes the relationship between predicted confidence scores and observed frequencies, while the ECE quantifies the average discrepancy between them. To construct the reliability diagram and compute the ECE, we first partition $B = 10,000$ test samples into 10 equally spaced bins according to their predicted confidence scores. For each bin \mathcal{B}_j , the average predicted confidence $\text{conf}(\mathcal{B}_j)$ and the empirical accuracy $\text{acc}(\mathcal{B}_j)$ are calculated as follows:

$$\text{conf}(\mathcal{B}_j) = \frac{1}{|\mathcal{B}_j|} \sum_{i \in \mathcal{B}_j} \hat{p}_i, \quad (44)$$

$$\text{acc}(\mathcal{B}_j) = \frac{1}{|\mathcal{B}_j|} \sum_{i \in \mathcal{B}_j} \mathbb{1}(l_i = \hat{l}_i), \quad (45)$$

where \hat{p}_i denotes the predicted confidence score for sample i , \hat{l}_i is the predicted label, and l_i is the ground-truth label.

In the reliability diagram, the empirical accuracy $\text{acc}(\mathcal{B}_j)$ for each bin $j \in 0, 1, \dots, 9$ is plotted against the corresponding average predicted confidence. The ECE is defined as

$$\text{ECE} = \sum_{j=0}^9 \frac{|\mathcal{B}_j|}{B} |\text{acc}(\mathcal{B}_j) - \text{conf}(\mathcal{B}_j)|. \quad (46)$$

Figure 6 presents the reliability diagrams and ECEs of the models trained with the proposed and benchmark FL methods under the default simulation setup, as detailed in Tables I and II. It is observed that the benchmark FL methods, which are based on a frequentist learning approach, exhibit large gaps

between the bars and the diagonal. In particular, the frequentist approach tends to produce overconfident predictions, as indicated by these gaps. In contrast, the proposed framework achieves noticeably smaller gaps than the benchmark methods, owing to its distribution-level aggregation and probabilistic inference. Furthermore, the proposed method attains an ECE that is nearly half of that of the benchmark methods.

VII. CONCLUSION

In this paper, we proposed a novel distribution-level AirComp framework specifically designed to address the challenges faced by FL in wireless edge networks characterized by data scarcity and heterogeneity. By leveraging Bayesian inference, our approach effectively captures model uncertainty through the maintenance of posterior distributions, significantly reducing local overfitting and client drift. Unlike conventional FL methods that rely on simple averaging, the proposed Bayesian aggregation framework performs efficient distribution-level conflation of local posteriors over wireless channels by exploiting the superposition property of analog AirComp. Within this framework, we developed an optimal transmit power control strategy grounded in rigorous convergence analysis, explicitly accounting for practical wireless impairments such as channel fading and noise. The analysis revealed that, under constrained power budgets, update distortion becomes the dominant factor limiting convergence. Extensive simulations validated our approach, demonstrating substantial improvements in test accuracy and robustness across various wireless scenarios compared to conventional FL methods including FedAvg, FedProx, and SCAFFOLD. In addition, the proposed framework achieved superior calibration performance, reducing ECE by nearly 50% relative to the conventional FL methods. This capability is crucial in safety-critical applications where reliable confidence estimation is as important as predictive accuracy. Our framework thus provides a robust, communication-efficient, and reliable solution for practical wireless FL deployments, especially beneficial in scenarios with limited and non-i.i.d. data.

APPENDIX A
PROOF OF THEOREM 1

For simplicity, we consider $E = 1$ and $d = F$, which implies $N_1 = N_2 = 1$. Consequently, the superscripts (n_1) and (n_2) that denote the OFDM symbol indices are omitted in the subsequent convergence analysis. Under Assumption 1, the decrease in the cost function during the first phase of training round t is bounded above as

$$\begin{aligned}
& L(\boldsymbol{\nu}_t, \boldsymbol{\rho}_{t+1}) - L(\boldsymbol{\nu}_t, \boldsymbol{\rho}_t) \\
& \leq \nabla_{\rho} L(\boldsymbol{\nu}_t, \boldsymbol{\rho}_t)^{\top} (\boldsymbol{\rho}_{t+1} - \boldsymbol{\rho}_t) + \frac{\Lambda_{\rho}}{2} \|\boldsymbol{\rho}_{t+1} - \boldsymbol{\rho}_t\|^2 \\
& \stackrel{(a)}{=} \nabla_{\rho} L(\boldsymbol{\mu}_t, \boldsymbol{\rho}_t)^{\top} \left(-\eta \sum_{k \in \mathcal{K}} \pi_k \nabla_{\rho} L_k(\boldsymbol{\mu}_t, \boldsymbol{\rho}_t) + \eta \boldsymbol{\xi}_{\rho_t} + \mathbf{z}'_{\rho_t} \right) \\
& \quad + \frac{\Lambda_{\rho}}{2} \left\| -\eta \sum_{k \in \mathcal{K}} \pi_k \nabla_{\rho} L_k(\boldsymbol{\mu}_t, \boldsymbol{\rho}_t) + \eta \boldsymbol{\xi}_{\rho_t} + \mathbf{z}'_{\rho_t} \right\|^2 \\
& = -\eta \|\nabla_{\rho} L(\boldsymbol{\mu}_t, \boldsymbol{\rho}_t)\|^2 + \nabla_{\rho} L(\boldsymbol{\mu}_t, \boldsymbol{\rho}_t)^{\top} (\eta \boldsymbol{\xi}_{\rho_t} + \mathbf{z}'_{\rho_t}) \\
& \quad + \frac{\Lambda_{\rho}}{2} \left\| -\eta \nabla_{\rho} L(\boldsymbol{\mu}_t, \boldsymbol{\rho}_t) + \eta \boldsymbol{\xi}_{\rho_t} + \mathbf{z}'_{\rho_t} \right\|^2, \tag{47}
\end{aligned}$$

where the equality (a) comes from the fact that $\boldsymbol{\Delta}_{\rho_{t,k}} = -\eta \nabla_{\rho} \frac{L_k(\boldsymbol{\nu}_t, \boldsymbol{\rho}_t)}{\delta}$ for $E = 1$, and $\mathbf{z}'_{\rho_t} \sim \mathcal{CN}(0, \frac{\delta \rho_t \sigma_z^2}{\gamma} \mathbf{I}_d)$. Using (47), the expected decrease in the cost function over channel noise is upper bounded as

$$\begin{aligned}
& \mathbb{E}_{\mathbf{z}} [L(\boldsymbol{\nu}_t, \boldsymbol{\rho}_{t+1}) - L(\boldsymbol{\nu}_t, \boldsymbol{\rho}_t)] \\
& \leq -\eta \|\nabla_{\rho} L(\boldsymbol{\mu}_t, \boldsymbol{\rho}_t)\|^2 + \eta \nabla_{\rho} L(\boldsymbol{\mu}_t, \boldsymbol{\rho}_t)^{\top} \boldsymbol{\xi}_{\rho_t} \\
& \quad + \frac{\Lambda_{\rho}}{2} \left\| -\eta \nabla_{\rho} L(\boldsymbol{\mu}_t, \boldsymbol{\rho}_t) + \eta \boldsymbol{\xi}_{\rho_t} \right\|^2 + \frac{\Lambda_{\rho} d \bar{\delta}_{\rho_t} \sigma_z^2}{2\gamma} \\
& \leq -\eta \|\nabla_{\rho} L(\boldsymbol{\mu}_t, \boldsymbol{\rho}_t)\|^2 + \eta \nabla_{\rho} L(\boldsymbol{\mu}_t, \boldsymbol{\rho}_t)^{\top} \boldsymbol{\xi}_{\rho_t} \\
& \quad + \frac{\Lambda_{\rho} \eta^2}{2} \left(\|\nabla_{\rho} L(\boldsymbol{\mu}_t, \boldsymbol{\rho}_t)\|^2 + \|\boldsymbol{\xi}_{\rho_t}\|^2 \right) + \frac{\Lambda_{\rho} d \bar{\delta}_{\rho_t} \sigma_z^2}{2\gamma} \\
& \stackrel{(a)}{\leq} -\eta \|\nabla_{\rho} L(\boldsymbol{\mu}_t, \boldsymbol{\rho}_t)\|^2 + \frac{\eta}{2} \left(\|\nabla_{\rho} L(\boldsymbol{\mu}_t, \boldsymbol{\rho}_t)\|^2 + \|\boldsymbol{\xi}_{\rho_t}\|^2 \right) \\
& \quad + \frac{\Lambda_{\rho} \eta^2}{2} \left(\|\nabla_{\rho} L(\boldsymbol{\mu}_t, \boldsymbol{\rho}_t)\|^2 + \|\boldsymbol{\xi}_{\rho_t}\|^2 \right) + \frac{\Lambda_{\rho} d \bar{\delta}_{\rho_t} \sigma_z^2}{2\gamma} \\
& = -\frac{\eta}{2} (1 - \Lambda_{\rho} \eta) \|\nabla_{\rho} L(\boldsymbol{\mu}_t, \boldsymbol{\rho}_t)\|^2 + \frac{\eta}{2} (1 + \Lambda_{\rho} \eta) \|\boldsymbol{\xi}_{\rho_t}\|^2 \\
& \quad + \frac{\Lambda_{\rho} d \bar{\delta}_{\rho_t} \sigma_z^2}{2\gamma}, \tag{48}
\end{aligned}$$

where the inequality (a) comes from the inequality of arithmetic and geometric means.

Using the updated global covariance matrix $\boldsymbol{\Sigma}_{t+1} = \text{diag}(\boldsymbol{\rho}_{t+1}^{-1})$, an upper bound on the decrease in the cost function during the second phase can be derived similarly to (47), as

$$\begin{aligned}
& L(\boldsymbol{\nu}_{t+1}, \boldsymbol{\rho}_{t+1}) - L(\boldsymbol{\nu}_t, \boldsymbol{\rho}_{t+1}) \\
& \leq \nabla_{\nu} L(\boldsymbol{\nu}_t, \text{diag}(\boldsymbol{\Sigma}_{t+1}^{-1}))^{\top} (\boldsymbol{\nu}_{t+1} - \boldsymbol{\nu}_t) + \frac{\Lambda_{\nu}}{2} \|\boldsymbol{\nu}_{t+1} - \boldsymbol{\nu}_t\|^2 \\
& = -\eta \|\nabla_{\nu} L(\boldsymbol{\nu}_t, \text{diag}(\boldsymbol{\Sigma}_{t+1}^{-1}))\|^2 + \nabla_{\nu} L(\boldsymbol{\nu}_t, \text{diag}(\boldsymbol{\Sigma}_{t+1}^{-1}))^{\top} \\
& \quad \times (\eta \boldsymbol{\xi}_{\nu_t} + \mathbf{z}'_{\nu_t}) + \frac{\Lambda_{\nu}}{2} \left\| -\eta \nabla_{\nu} L(\boldsymbol{\nu}_t, \text{diag}(\boldsymbol{\Sigma}_{t+1}^{-1})) + \eta \boldsymbol{\xi}_{\nu_t} + \mathbf{z}'_{\nu_t} \right\|^2. \tag{49}
\end{aligned}$$

From (49), the expected decrease in the cost function over channel noise can be derived in a manner similar to (48), as

$$\begin{aligned}
& \mathbb{E}_{\mathbf{z}} [L(\boldsymbol{\nu}_t, \text{diag}(\boldsymbol{\Sigma}_{t+1}^{-1})) - L(\boldsymbol{\nu}_t, \text{diag}(\boldsymbol{\Sigma}_{t+1}^{-1}))] \\
& \leq -\frac{\eta}{2} (1 - \Lambda_{\nu} \eta) \|\nabla_{\nu} L(\boldsymbol{\nu}_t, \text{diag}(\boldsymbol{\Sigma}_{t+1}^{-1}))\|^2 \\
& \quad + \frac{\eta}{2} (1 + \Lambda_{\nu} \eta) \|\boldsymbol{\xi}_{\nu_t}\|^2 + \frac{\Lambda_{\nu} d \bar{\delta}_{\nu_t} \sigma_z^2}{2\gamma}. \tag{50}
\end{aligned}$$

Set $\eta = \frac{1}{\sqrt{T}}$, and extend the expectation over randomness in the trajectory across T training rounds as follows:

$$\begin{aligned}
& \mathbb{E}[L(\boldsymbol{\nu}_0, \boldsymbol{\rho}_0) - L(\boldsymbol{\nu}_T, \boldsymbol{\rho}_T)] = \mathbb{E} \left[\sum_{t=0}^{T-1} L(\boldsymbol{\nu}_t, \boldsymbol{\rho}_t) - L(\boldsymbol{\nu}_{t+1}, \boldsymbol{\rho}_{t+1}) \right] \\
& = \mathbb{E} \left[\sum_{t=0}^{T-1} L(\boldsymbol{\nu}_t, \boldsymbol{\rho}_t) - L(\boldsymbol{\nu}_t, \boldsymbol{\rho}_{t+1}) \right. \\
& \quad \left. + L(\boldsymbol{\nu}_t, \boldsymbol{\rho}_{t+1}) - L(\boldsymbol{\nu}_{t+1}, \boldsymbol{\rho}_{t+1}) \right] \\
& \stackrel{(a)}{\geq} \mathbb{E} \left[\sum_{t=0}^{T-1} \frac{1}{2\sqrt{T}} \left(1 - \frac{\Lambda_{\rho}}{\sqrt{T}} \right) \|\nabla_{\rho} L(\boldsymbol{\mu}_t, \boldsymbol{\rho}_t)\|^2 \right. \\
& \quad - \frac{1}{2\sqrt{T}} \left(1 + \frac{\Lambda_{\rho}}{\sqrt{T}} \right) \|\boldsymbol{\xi}_{\rho_t}\|^2 - \frac{\Lambda_{\rho} d \bar{\delta}_{\rho_t} \sigma_z^2}{2\gamma} \\
& \quad \left. + \frac{1}{2\sqrt{T}} \left(1 - \frac{\Lambda_{\nu}}{\sqrt{T}} \right) \|\nabla_{\nu} L(\boldsymbol{\nu}_t, \text{diag}(\boldsymbol{\Sigma}_{t+1}^{-1}))\|^2 \right. \\
& \quad \left. - \frac{1}{2\sqrt{T}} \left(1 + \frac{\Lambda_{\nu}}{\sqrt{T}} \right) \|\boldsymbol{\xi}_{\nu_t}\|^2 - \frac{\Lambda_{\nu} d \bar{\delta}_{\nu_t} \sigma_z^2}{2\gamma} \right] \\
& \stackrel{(b)}{=} \frac{1}{2\sqrt{T}} \mathbb{E} \left[\sum_{t=0}^{T-1} \left(1 - \frac{\Lambda_{\rho}}{\sqrt{T}} \right) \|\nabla_{\rho} L(\boldsymbol{\mu}_t, \boldsymbol{\rho}_t)\|^2 \right. \\
& \quad \left. + \left(1 - \frac{\Lambda_{\nu}}{\sqrt{T}} \right) \|\nabla_{\nu} L(\boldsymbol{\nu}_t, \text{diag}(\boldsymbol{\Sigma}_{t+1}^{-1}))\|^2 \right. \\
& \quad \left. - \left(1 + \frac{\Lambda_{\rho}}{\sqrt{T}} \right) \|\boldsymbol{\xi}_{\rho_t}\|^2 - \left(1 + \frac{\Lambda_{\nu}}{\sqrt{T}} \right) \|\boldsymbol{\xi}_{\nu_t}\|^2 \right] \\
& \quad - \frac{\Lambda_{\rho} \sigma_z^2}{2\gamma} \mathbb{E} \left[\frac{1}{T} \sum_{t=0}^{T-1} \sum_{k \in \mathcal{K}} \pi_k \|\nabla_{\rho} L_k(\boldsymbol{\mu}_t, \boldsymbol{\rho}_t)\|^2 \right] \\
& \quad - \frac{\Lambda_{\nu} \sigma_z^2}{2\gamma} \mathbb{E} \left[\frac{1}{T} \sum_{t=0}^{T-1} \sum_{k \in \mathcal{K}} \pi_k \|\nabla_{\nu} L_k(\boldsymbol{\nu}_t, \text{diag}(\boldsymbol{\Sigma}_{t+1}^{-1}))\|^2 \right] \\
& = \frac{1}{2\sqrt{T}} \mathbb{E} \left[\sum_{t=0}^{T-1} \left(1 - \frac{\Lambda_{\rho}}{\sqrt{T}} \right) \|\nabla_{\rho} L(\boldsymbol{\mu}_t, \boldsymbol{\rho}_t)\|^2 \right. \\
& \quad \left. + \left(1 - \frac{\Lambda_{\nu}}{\sqrt{T}} \right) \|\nabla_{\nu} L(\boldsymbol{\nu}_t, \text{diag}(\boldsymbol{\Sigma}_{t+1}^{-1}))\|^2 \right] \\
& \quad - \frac{1}{2\sqrt{T}} \mathbb{E} \left[\sum_{t=0}^{T-1} \left(1 + \frac{\Lambda_{\rho}}{\sqrt{T}} \right) \|\boldsymbol{\xi}_{\rho_t}\|^2 + \left(1 + \frac{\Lambda_{\nu}}{\sqrt{T}} \right) \|\boldsymbol{\xi}_{\nu_t}\|^2 \right] \\
& \quad - \frac{\Lambda_{\rho} \sigma_z^2}{2\gamma T} \mathbb{E} \left[\sum_{t=0}^{T-1} \sum_{k \in \mathcal{K}} \pi_k \|\nabla_{\rho} L_k(\boldsymbol{\mu}_t, \boldsymbol{\rho}_t)\|^2 \right] \\
& \quad - \frac{\Lambda_{\nu} \sigma_z^2}{2\gamma T} \mathbb{E} \left[\sum_{t=0}^{T-1} \sum_{k \in \mathcal{K}} \pi_k \|\nabla_{\nu} L_k(\boldsymbol{\nu}_t, \text{diag}(\boldsymbol{\Sigma}_{t+1}^{-1}))\|^2 \right], \tag{51}
\end{aligned}$$

where the inequality (a) comes from (48) and (50), and the equality (b) comes from the fact that $\bar{\delta}_{\rho_t} = \sum_{k \in \mathcal{K}} \frac{\pi_k}{d} \|\eta \nabla_{\rho} L_k(\boldsymbol{\mu}_t, \boldsymbol{\rho}_t)\|^2$ and $\bar{\delta}_{\nu_t} = \sum_{k \in \mathcal{K}} \frac{\pi_k}{d} \|\eta \nabla_{\nu} L_k(\boldsymbol{\nu}_t, \text{diag}(\boldsymbol{\Sigma}_{t+1}^{-1}))\|^2$ for $E = 1$.

REFERENCES

- [1] B. McMahan, E. Moore, D. Ramage, S. Hampson, and B. A. Y. Arcas, "Communication-efficient learning of deep networks from decentralized data," in *Proc. Int. Conf. Artif. Intell. Stat.*, Apr. 2017.
- [2] Y. Zhao, M. Li, L. Lai, N. Suda, D. Civin, and V. Chandra, "Federated learning with non-iid data," arXiv preprint arXiv:1806.00582, 2018. [Online]. Available: <https://arxiv.org/abs/1806.00582>
- [3] T. Li, A. K. Sahu, M. Zaheer, M. Sanjabi, A. Talwalkar, and V. Smith, "Federated optimization in heterogeneous networks," in *Proc. Mach. Learn. Syst.*, Mar. 2020.
- [4] S. P. Karimireddy, S. Kale, M. Mohri, S. Reddi, S. Stich, and A. T. Suresh, "SCAFFOLD: Stochastic controlled averaging for federated learning," in *Proc. Int. Conf. Mach. Learn.*, Jul. 2020.
- [5] J. Wang, Q. Liu, H. Liang, G. Joshi, and H. V. Poor, "Tackling the objective inconsistency problem in heterogeneous federated optimization," in *Proc. Adv. Neural Inf. Process. Syst.*, Dec. 2020.
- [6] Q. Li, B. He, and D. Song, "Model-contrastive federated learning," in *Proc. IEEE/CVF Conf. Comput. Vis. Pattern Recognit.*, Jun. 2021.
- [7] D. A. E. Acar, Y. Zhao, R. Matas, M. Mattina, P. Whatmough, and V. Saligrama, "Federated learning based on dynamic regularization," in *Proc. Int. Conf. Mach. Learn.*, Jul. 2021.
- [8] M. Kamp, J. Fischer, and J. Vreeken, "Federated learning from small datasets," in *Proc. Int. Conf. Learn. Repr.*, May 2023.
- [9] L. Cao, H. Chen, X. Fan, J. Gama, Y.-S. Ong, and V. Kumar, "Bayesian federated learning: A survey," arXiv preprint arXiv:2304.13267, 2023. [Online]. Available: <https://arxiv.org/abs/2304.13267>
- [10] L. Liu, X. Jiang, H. Chen, G.-J. Qi, H. Huang, and L. Shao, "A Bayesian federated learning framework with online laplace approximation," *IEEE Trans. Pattern Anal. Mach. Intell.*, vol. 46, no. 1, pp. 1–16, Jan. 2024.
- [11] M. M. Amiri and D. Gunduz, "Federated learning over wireless fading channels," *IEEE Trans. Wireless Commun.*, vol. 19, no. 5, pp. 3546–3557, May 2020.
- [12] G. Zhu, Y. Wang, and K. Huang, "Broadband analog aggregation for low-latency federated edge learning," *IEEE Trans. Wireless Commun.*, vol. 19, no. 1, pp. 491–504, Jan. 2020.
- [13] J.-P. Hong, S. Park, and W. Choi, "Base station dataset-assisted broadband over-the-air aggregation for communication-efficient federated learning," *IEEE Trans. Wireless Commun.*, vol. 22, no. 11, pp. 7259–7272, Nov. 2023.
- [14] —, "Over-the-air aggregation-based federated learning in cache-enabled wireless edge networks," in *Proc. IEEE Int. Conf. Commun.*, Rome, Italy, May/June 2023.
- [15] X. Cao, G. Zhu, J. Xu, Z. Wang, and S. Cui, "Optimized power control design for over-the-air federated edge learning," *IEEE J. Sel. Areas Commun.*, vol. 40, no. 1, p. 342–358, Jan. 2022.
- [16] X. Cao, G. Zhu, J. Xu, and K. Huang, "Optimized power control for over-the-air computation in fading channels," *IEEE Trans. Wireless Commun.*, vol. 19, no. 11, p. 7498–7513, Nov. 2020.
- [17] G. Zhu, Y. Du, D. Gunduz, and K. Huang, "One-bit over-the-air aggregation for communication-efficient federated edge learning: Design and convergence analysis," *IEEE Trans. Wireless Commun.*, vol. 20, no. 3, p. 2120–2135, Mar. 2021.
- [18] B. Kim, H. Seo, and W. Choi, "Privacy-enhanced over-the-air federated learning via client-driven power balancing," arXiv preprint arXiv:2410.05907, 2024. [Online]. Available: <https://arxiv.org/abs/2410.05907>
- [19] T. Gafni, K. Cohen, and Y. C. Eldar, "Federated learning from heterogeneous data via controlled bayesian air aggregation," arXiv preprint arXiv:2303.17413, 2023. [Online]. Available: <https://arxiv.org/abs/2303.17413>
- [20] C. Park, S. Lee, and N. Lee, "Bayesian aircomp with sign-alignment precoding for wireless federated learning," in *Proc. IEEE Int. Conf. Commun.*, Jun. 2021.
- [21] Y. Shao, D. Gunduz, and S. C. Liew, "Bayesian over-the-air computation," *IEEE J. Sel. Areas Commun.*, vol. 41, no. 3, pp. 589–606, Mar. 2023.
- [22] A. Graves, "Practical variational inference for neural networks," in *Proc. Adv. Neural Inf. Process. Syst.*, 2011.
- [23] C. Blundell, J. Cornebise, K. Kavukcuoglu, and D. Wierstra, "Weight uncertainty in neural networks," in *Proc. Int. Conf. Mach. Learn.*, 2015.
- [24] H. Seo, Y. Kang, M. Bennis, and W. Choi, "Bayesian inverse contextual reasoning for heterogeneous semantics- native communication," *IEEE Trans. Commun.*, vol. 72, no. 2, pp. 830–844, 2024.
- [25] T. P. Hill, "Conflations of probability distributions," *Trans. Amer. Math. Soc.*, vol. 363, no. 6, pp. 3351–3372, Jun. 2011.
- [26] A. Özer, K. B. Buldu, A. Akgül, and G. Unal, "How to combine variational bayesian networks in federated learning," in *Proc. Adv. Neural Inf. Process. Syst. Workshop*, Dec. 2022.
- [27] X. Zhang, W. Li, Y. Shao, and Y. Li, "Federated learning via variational bayesian inference: Personalization, sparsity and clustering," arXiv preprint arXiv:2303.04345, 2023. [Online]. Available: <https://arxiv.org/abs/2303.04345>
- [28] P. Esposito, "Blitz - bayesian layers in torch zoo (a bayesian deep learning library for torch)," *GitHub repository*, 2020.
- [29] C. Guo, G. Pleiss, Y. Sun, and K. Q. Weinberger, "On calibration of modern neural networks," in *Proc. Int. Conf. Mach. Learn.*, 2017, pp. 1321–1330.